Hindawi
International Journal of Corrosion
Volume 2022, Article ID 6681008, 12 pages
https://doi.org/10.1155/2022/6681008

*Research Article*

# In Situ Monitoring of Corrosion under Insulation Using Electrochemical and Mass Loss Measurements

**Mingzhang Yang and Jing Liu**

*Department of Chemical and Materials Engineering, University of Alberta, Edmonton, Alberta, Canada T6G 1H9*

Correspondence should be addressed to Jing Liu; jing.liu.arrow@ualberta.ca

Received 8 November 2020; Revised 12 August 2021; Accepted 3 December 2021; Published 10 January 2022

Academic Editor: Xun Xi



Corrosion under insulation (CUI) refers to the external corrosion of piping and vessels when they are encapsulated in thermal insulation. To date, very limited information (especially electrochemical data) is available for these "difficult-to-test" CUI conditions. This study was aimed at developing a novel electrochemical sensing method for in situ CUI monitoring and analysis. Pt-coated Ti wires were used to assemble a three-electrode electrochemical cell over a pipe surface covered by thermal insulation. The CUI behavior of X70 carbon steel (CS) and 304 stainless steel (SS) under various operating conditions was investigated using mass loss, linear polarization resistance (LPR), and electrochemical impedance spectroscopy (EIS) measurements. It was found that both the consecutive wet and dry cycles and cyclic temperatures accelerated the progression of CUI. LPR and EIS measurements revealed that the accelerated CUI by thermal cycling was due to the reduced polarization resistance and deteriorated corrosion film. Enhanced pitting corrosion was observed on all tested samples after thermal cycling conditions, especially for CS samples. The proposed electrochemical technique demonstrated the ability to obtain comparable corrosion rates to conventional mass loss data. In addition to its potential for in situ CUI monitoring, this design could be further applied to rank alloys, coatings, and inhibitors under more complex exposure conditions.

## 1. Introduction

Corrosion under insulation (CUI) is a corrosion issue and a major integrity problem in petrochemical industry. Thermal insulation is primarily utilized on piping, vessels, and tanks to reduce heat loss and prevent condensation on steel surfaces having temperatures below the dew point of the surrounding atmosphere [1]. Over time, atmospheric moisture (e.g., rain and fog) can penetrate the insulation and be trapped in the gap between insulation and steel surface, eventually leading to CUI of the steel [2]. Due to the accumulation of trapped water and contaminants, CUI is generally more aggressive than the external corrosion of uninsulated metals [3]. The equipment failure caused by CUI can have catastrophic effects on production, safety, and environment. As an example, the leaks in a 4-in hydrocarbon line caused by CUI led to a massive fire that cost the company US$ 50 million [1]. Additionally, the presence of insulation allows the undetected progression of CUI. Companies rarely have enough budget for regular in-service inspections, scheduled maintenance, and records to keep up with CUI failures. A report by ExxonMobil in 2003 showed that 40 to 60% of piping maintenance costs are related to CUI [1].

The progression of CUI involves many factors, including insulation types, coating materials, substrate materials, and operating conditions [4, 5]. Among these factors, extensive efforts were made to select the optimum insulation and/or coating materials with excellent CUI resistance in various service environments, while the stability/durability of substrate materials under various operating conditions still requires further investigation [6–10]. Javaherdashti suggested that an inappropriate combination of substrate materials and operating conditions could be very risky [1]. X70 carbon steel (CS) and 300 series stainless steel (SS) are the most widely used materials for piping and vessels. Due to their difference in chemistry and microstructure, CUI of CS can be normally manifested as general and localized

corrosion at temperatures between −4 and 149°C, while CUI of SS can become susceptible to stress corrosion cracking and pitting corrosion between 49°C and 149°C [1, 3, 11, 12]. Research has shown the CUI to be the worst at around 93°C for both types of steel [3]. In addition to thermal conditions, wet/dry cycles have also been deemed important with regard to CUI. For instance, wet/dry cycles near the working temperature below the dew point can increase the concentration of chlorine and sulfur beneath the insulation and facilitate the corrosion rate [3].

CUI inspection in the field requires a complicated and time-consuming process. Existing techniques, such as visual inspection, infrared testing, radiography, moisture detectors, and/or removers, either require the removal of insulation and cladding or cannot give a direct and reliable indication of the corrosion status of the materials [8, 13–15]. ASTM standard (G189-07) for laboratory simulation of CUI includes a provision for using a potentiostat to conduct electrochemical polarization resistance measurement under isothermal/cyclic temperature and wet/dry conditions simulating desired conditions in service [16]. However, this design has the drawback of using noninert materials (e.g., alloys or coatings) as the counter electrode (CE) and reference electrode (RE), which may lead to unrealistic electrochemical results [17]. The existing commercial REs (e.g., Ag/AgCl, $Cu/CuSO_4$, and $Hg/HgSO_4$) and CEs (e.g., Pt, graphite, and glassy carbon) are either not robust (easily damaged) or uneconomical to be used in the field. Thus, there is not only a lack of understanding on the CUI performance of alloys under various conditions (e.g., cyclic wet/dry temperature) but also a lack of practical electrochemical techniques for in situ (in-line) CUI monitoring.

This study is aimed at developing an electrochemical method to investigate the CUI behavior of steels under various operating conditions (i.e., isothermal/cyclic temperature and wet/dry conditions). For this attempt, a CUI apparatus based on the ASTM G189 recommendation for CUI simulation was built [16]. The in situ CUI monitoring and analysis were achieved using a novel electrochemical assembly with three Pt-coated titanium (noted as Pt(Ti)) wires as the sensing electrodes. The CUI behaviors of the two most widely used substrate materials, X70 CS and 304 SS, were studied using the mass loss data, electrochemical measurements, and surface characterization.

## 2. Materials and Experiment

*2.1. Materials and Sample Preparation.* The chemical composition of used X70 CS and 304 SS, is shown in Table 1. Both CS and SS ring specimens were cut from seamless tubing with an outer diameter and a thickness of 89 mm and 10 mm, respectively. Prior to installation, the exposed surfaces of each substrate material (area 28.0 $cm^2$) were abraded using successive grades of SiC papers down to 600 grit, thoroughly cleaned with deionized (DI) water, ultrasonically washed in ethanol for 5 min, and dried. The initial weights of these samples were measured using an analytical balance with an accuracy of 0.1 mg. The insulation material used was mineral wool with conductivity and density of $0.044\,W\,m^{-1}\,K^{-1}$ and $128\,kg\,m^{-3}$. 0.01 wt% and 3.5 wt% NaCl testing solutions were selected to represent industrial and coastal environments that contain atmosphere condensate with impurities of chlorides [18, 19]. NaCl solutions were prepared with DI water under naturally aerated conditions.

Table 1: The nominal compositions of X70 CS and 304 SS specimens used in this study.

| | Elements (wt%) | | | | | | |
|---|---|---|---|---|---|---|---|
| Material | C | Mn | P | Cr | Ni | Ti | Fe |
| CS | 0.043 | 1.29 | 0.01 | — | — | 0.025 | Bal. |
| SS | 0.029 | 1.11 | 0.01 | 18.6 | 8.13 | — | Bal. |

*2.2. Experimental Setups.* Two distinctive apparatuses were designed to evaluate the CUI with different materials and conditions: (i) mass loss evaluation of CS in 0.01 wt% NaCl solution (Figure 1(a)) and (ii) electrochemical investigation of CUI in 3.5 wt% NaCl solution (Figure 1(b)). Both apparatuses were based on ASTM G189-07 [16].

*2.2.1. Mass Loss Evaluation of CS.* Figure 1(a) presents the schematic of the mass loss apparatus. The test rig consists of six ring specimens separated by insulation spacers made of polytetrafluoroethylene (PTFE): three on the left portion and three on the right portion. The CUI cell on the left portion was used to simulate constant wet conditions: isothermal wet (IW) and cyclic wet (CW), while the right portion was used to simulate the wet and dry conditions: isothermal wet and dry (IWD) and cyclic wet and dry (CWD). An immersion heater and a thermocouple controlled the temperature of these ring specimens. Mineral wool was wrapped around the outside of the evaluation sections to create thermal insulation and annular space (31.1 $cm^3$ per specimen) to retain test solutions. An aluminum foil jacket was then slid over the insulation for setup fixation. Each CUI cell has an opening (6 mm) at 12 o'clock position and a drain hole (6 mm) at 6 o'clock position.

Testing conditions and duration associated with Figure 1(a) are summarized in Table 2. 0.01 wt% NaCl solution was chosen as the testing electrolyte according to ASTM G189-07 [16]. The wet cycle was maintained by pumping solution at a rate of 2 mL/min via the openings at 12 o'clock position. The dry cycle of IWD and CWD conditions was achieved by opening the drain holes at six (6) o'clock position to drain the trapped solution and moisture with a four-(4-) hour drying time every 24 hours.

*2.2.2. Electrochemical Investigation of CUI.* Figure 1(b) presents the novel electrochemical dual CUI cell for both electrochemical and mass loss measurements. Instead of using CS as substrate materials for both cells, four CS and four SS ring specimens were separated into two cells. For validation purposes, two rings in each set of four specimens were used as the working electrodes (WEs). This allows each electrochemical measurement to be repeated. The other two rings of each cell were simply used for mass loss

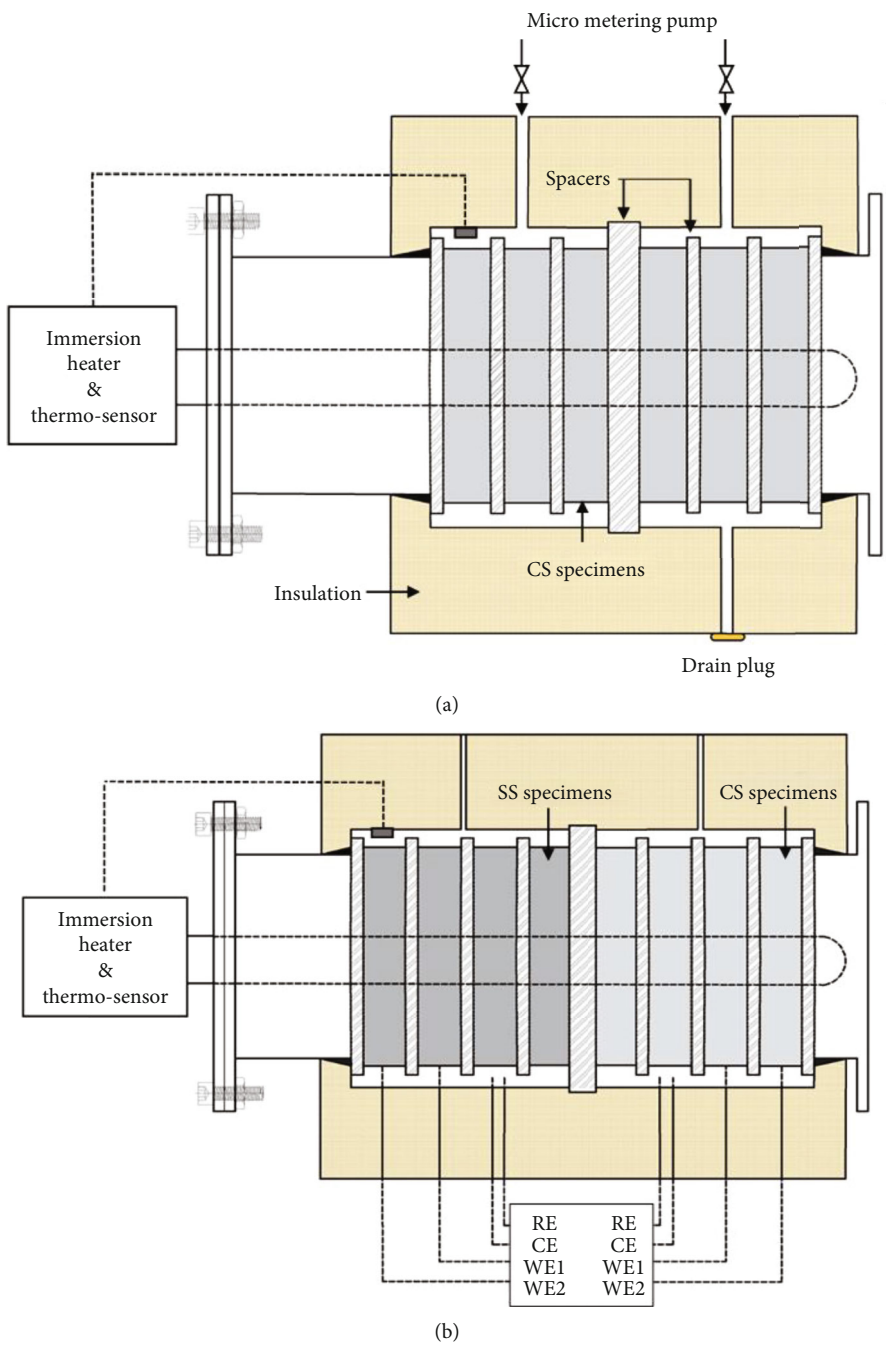


Figure 1: Schematic overview of the two dual CUI cells: (a) mass loss dual cell with the left side for constant wet condition *vs*. right side with a robust drain plug for wet and dry conditions; (b) electrochemical dual cell with CS samples (left) *vs*. SS samples (right).

measurement; therefore, they were not connected to the potentiostat as WEs.

Figure 2 illustrates the arrangement for WE, CE, and RE under the thermal insulation. An insulated Pt(Ti) wire with a bare tip (i.e., active surface made of Pt(Ti)) was isolated from the testing solution by connecting it to the inner wall of the ring specimens (i.e., WEs). Instead of using spare ring specimens such as CE and RE as suggested by ASTM G189-07, insulated Pt(Ti) wires with bare tips were utilized as CE and RE. The bare tips of CE and RE were hanging in the annular space between metal and insulation where the electrolyte was retained. This design was inspired by a patent, where three insulated Pt wires were used as the oxidation-reduction potential (ORP) sensors (i.e., WE, RE, and CE) in hot acidic solutions [20]. Pt(Ti) wires with lower cost and better strength were used in this study instead of pure Pt wires to cater for future field applications.

Testing conditions and duration associated with Figure 1(b) are summarized in Table 3. 3.5 wt% NaCl solution was used as the electrolyte to resemble a marine or

Table 2: CUI testing matrix for mass loss evaluation of CS in 0.01 wt% NaCl solutions.

| Condition code | $T$ (°C) | Cycle (h) | Duration (days) | Dry cycle/24 h | Substrate materials |
|---|---|---|---|---|---|
| IW | 50 | 24 h-50°C | 7 | 0 h-dry | CS |
| | 93 | 24 h-93°C | 7 | 0 h-dry | CS |
| CW | 93-50 | 24 h-93°C/24 h-50°C | 7 | 0 h-dry | CS |
| IWD | 50 | 24 h-50°C | 7 | 4 h-dry | CS |
| | 93 | 24 h-93°C | 7 | 4 h-dry | CS |
| CWD | 93-50 | 24 h-93°C/24 h-50°C | 7 | 4 h-dry | CS |

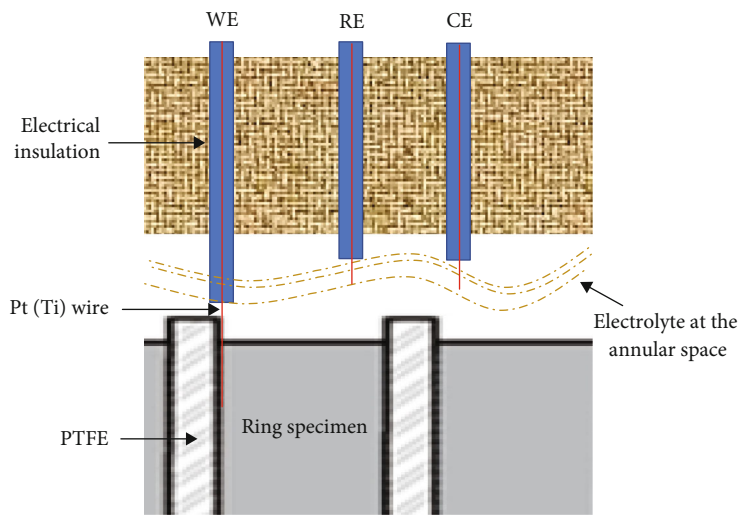


Figure 2: Schematic of the interface of electrodes, electrolyte, and ring specimens within the test cell.

Table 3: CUI test matrix for electrochemical investigation in 3.5 wt% NaCl solutions.

| Condition code | $T$ (°C) | Cycle (h) | Duration (days) | Substrate materials |
|---|---|---|---|---|
| IW | 93 | 24 h-93°C | 7 | SS, CS |
| CW | 93-50 | 24 h-93°C/ 24 h-50°C | 7 | SS, CS |

coastal environment [20]. The insulation was constantly kept wet by pumping solution at a rate of 2 mL/min via the openings at the 12 o'clock position.

Linear polarization resistance (LPR) and electrochemical impedance spectroscopy (EIS) experiments were conducted to study the CUI rates of SS and CS under different thermal conditions. The potentiostat used was a Princeton Applied Research VersaSTAT 3F. LPR experiments were performed from −20 mV to +20 mV *vs.* OCP (open circuit potential) with a scan rate of 0.5 mV $s^{-1}$ after one- (1-) hour of OCP measurement daily. The day 0 LPR measurements were done right after the initiation of CUI testing; day 1-7 LPR measurements were done at the end of day 1 to day 7. Three LPR curves were obtained for each specimen at same thermal and wet/dry condition for reproducibility. EIS measurements were performed at the OCP after the LPR measurements to characterize the passive films formed on samples. Measurements were conducted on the 3rd, 5th, and 7th days to avoid measuring before a steady state (e.g., day 1). The EIS perturbation voltage amplitude was 10 mV (peak-to-peak). The frequency range for all experiments was 0.01 Hz to 100 kHz with sampling at 10 points per decade.

### 2.3. Corrosion Rate Calculation

*2.3.1. Corrosion Rate Calculation by Mass Loss Data.* At the end of each experiment, the CUI cell including samples and insulation were dissembled. Samples were ultrasonically washed for 5 min in DI water and dried in air, and the final mass was measured. The treatment mentioned above was repeated to completely remove corrosion products according to the procedures given in ASTM G1-03 standard [21]. The formation of iron oxides is assumed to be negligible compared to the amount that spalling off and dissolved into solution. Average corrosion rate (CR) was calculated by incorporating the average mass loss of three samples which was then determined by equation (1) according to ASTM standard G31-72 [22]:

$$\mathrm{CR(mm/y)} = \frac{\Delta W \times K}{T \times A \times \rho}, \quad (1)$$

where $\Delta W$ is the average mass loss in g, $T$ is the exposure

time in h, $A$ is the exposure area (28.0 $cm^2$), $\rho$ is the density (8.02 g $cm^{-3}$ for SS and 7.87 g $cm^{-3}$ for CS, respectively), and $K$ is a CR constant ($8.76 \times 10^4$ h mm $y^{-1}$ $cm^{-1}$).

*2.3.2. Corrosion Rate Calculations by Polarization Resistance.* To quantitatively compare the LPR measurements with mass loss data, the CRs of WEs were calculated using equations (2) to (4) [23]:

$$\mathrm{CR(mm/y)} = C \bullet \frac{M i_{\mathrm{corr}}}{n\rho}, \tag{2}$$

$$i_{\mathrm{corr}} = \frac{B}{R_{\mathrm{p}}}, \tag{3}$$

where $i_{\mathrm{corr}}$ is the current density in $\mu$A $cm^{-2}$, $C$ is a constant that includes $F$ and any other conversion factor in mm $y^{-1}$ ($C = 3.27 \times 10^{-3}$ s mm mol $y^{-1}$ $cm^{-1}$), $M$ is the atomic mass equal to 55.85 g $mol^{-1}$, $\rho$ is the density in g $cm^{-3}$, and $n$ is the valence state of Fe and has been assumed to be 3+ for Fe in both the oxide film and solutions. $B$ is the Stern-Geary constant and is approximately 0.026 V in this work [17]; the polarization resistance, $R_{\mathrm{p}}$, of measuring electrode was determined as a slope of the fitted potential ($E$) *vs.* current density ($i$) according to [24]

$$R_{\mathrm{p}} = \left(\frac{\partial \Delta E}{\partial i}\right)_{i=0, dE/dt \longrightarrow 0}. \tag{4}$$

*2.4. Surface Characterizations.* The cross-sectional corroded CS samples were characterized for pits and corrosion product layers using a Leica DMIRM optical microscope (OM). A Tescan Vega3 scanning electron microscope (SEM) was used to observe the pit surface morphologies of the corroded SS specimens after CUI experiments.

## 3. Results and Discussion

*3.1. Effect of Various Thermal Cycling and Wet-Dry Cycling Conditions on the CUI Behavior of CS.* To evaluate the effect of thermal cycling and wet-dry cycling on the CUI behavior of CS, mass loss data were collected after seven (7) days of CUI experiments with 0.01 wt% NaCl solution. The obtained mass loss data were converted into area-normalized CRs using equation (1). Figure 3 presents the calculated CRs of CS samples under IW, IWD, CW, and CWD conditions.

As shown in Figure 3, the CRs present a tendency of cyclic 93-50°C > isothermal 93°C > isothermal 50°C for both constant wet and cyclic wet-dry conditions. Mizushima et al. suggested that increasing operating temperature, particularly between the ranges of 49 and 93°C, can speed up the electrochemical reactions and aggravate the subsequent mass loss [4]. Results in Figure 3 confirm Mizushima et al.'s conclusion, i.e., CR of CS at IW 93°C > IW 50°C and CR at IWD 93°C > IWD 50°C. Ashbaugh et al. proposed that the mechanism behind the accelerated CRs in substrate materials can be attributed to the accumulation of corrosive species on the metal surface as water evaporates [18]. The CS showed significant signs of degradation under cyclic 93-50°C conditions, with the CRs being more than twice that of its isothermal counterparts (i.e., isothermal 50°C and 93°C). This can be attributed to the combined effects of decohesion/spalling of oxide scales in response to thermal shock and the formation of condensation from thermal cycling. Both phenomena enhanced the CR, as the damaged oxide film exposed the bare metal surface, and the condensation generally contained high concentrations of chlorides. To summarize the effect of thermal conditions on the CUI behavior of CS in 0.01 wt% NaCl solutions, the cyclic temperature conditions studied were more aggressive than the isothermal conditions, and the isothermal conditions became more aggressive with increasing temperature. Specifically, CW 93-50°C > IW 93°C > IW 50°C, and CWD 93-50°C > IWD 93°C > IWD 50°C.

Similar to constant wet conditions, the most severe CUI under cyclic wet and dry condition was observed in the case of CWD, followed by IWD 93°C and IWD 50°C. In Figure 3, cyclic wet and dry conditions have shown higher mass loss results by factors of 5.2, 5.3, and 5.0 times under IW 50°C, IW 93°C, and CW 93-50°C, respectively. Previous studies have shown that CUI can be accelerated by consecutive wet and dry cycles, as they could result in a more aggressive electrolyte and higher localized concentration of oxygen after ventilation and drainage [8, 20]. Specifically, the installed mineral wool insulation absorbs moisture via capillary action, allowing the moisture to stay close to the substrate surface through surface tension [25]. During the dry cycle, a portion of liquid moisture will remain attached to the substrate surface. The attached liquid moisture contains higher concentrations of corrosive species (e.g., waterborne chlorides, sodium, and sulfates) leached from insulations, and those corrosive species enhanced both uniform and localized corrosion [1, 25, 26]. A recent study by Cao et al. found that the metallic ions leaching from mineral wool insulation ($Fe^{3+}$, $Ca^{2+}$, $Mg^{2+}$, and $K^+$) also lead to an increase in the electrolyte conductivity and subsequent higher kinetics of CUI [27]. Furthermore, the CUI rate is controlled by oxygen diffusion, because the main anodic and cathodic reactions of CUI are the oxidation of iron and the reduction of oxygen [20, 27, 28]. The dry cycle not only allows the solution to evaporate but also enhances the diffusion of oxygen to the insulation/metal interface, thereby accelerating the CR [8, 29]. The oxygen reduction reaction (i.e., $O_2 + 2H_2O + 4e^- \longrightarrow 4OH^-$) facilitates the passivation of steel and the formation of iron oxides (scales). However, the newly formed oxide scales (during 4 hours of dry cycle) can be easily destroyed by solution flushing during the wet cycle and cause more severe corrosion. In summary, on top of the effect of thermal conditions, CS samples corroded more rapidly in cyclic wet-dry than in constant wet with the same thermal condition, i.e., CWD > CW and IWD > IW.

*3.2. Electrochemical Investigation of the CUI Behavior of CS and SS.* To evaluate the effect of thermal cycling on the CUI of X70 CS and 304 SS, the samples were tested in 3.5 wt% NaCl solution using the designed electrochemical CUI cell (Figure 1(b)) under IW 93°C and CW 93-50°C

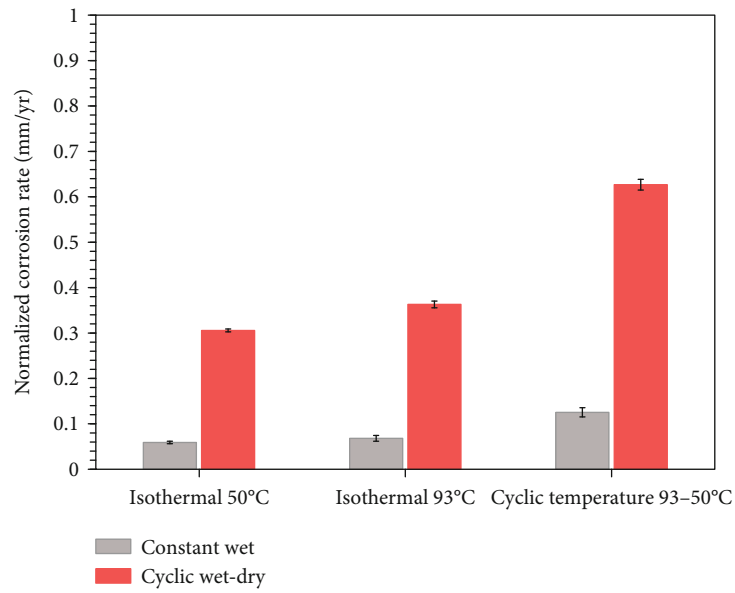


Figure 3: Normalized corrosion rates of carbon steels in 0.01 wt% NaCl solution under isothermal cycling, thermal cycling, and wet-dry cycling.

conditions for 7 days. The electrochemical and mass loss data were analyzed.

*3.2.1. Linear Polarization Resistance.* During 7-day CUI experiments, the LPR measurements were performed after one- (1-) hour OCP measurement from day 0 to day 7. The $R_p$ values were determined through equation (4) and are presented in Figure 4. Figures 4(a) and 4(b) present the $R_p$ *vs.* time of CS and SS samples, respectively. The circle and triangle symbols represent the data obtained in the 50°C and 93°C cycles of the CW 93-50°C test, respectively.

Figure 4(a) presents the $R_p$ *vs.* time of CS samples in 3.5 wt% NaCl solutions under IW 93°C and CW 93-50°C conditions. During the testing period (i.e., 7 days) at IW 93°C, CS exhibited a continuous decrease in $R_p$, suggesting its low corrosion resistance to the 3.5 wt% solution at 93°C. It can be seen that the $R_p$ of CS experienced an instant decline because the freshly clean CS surfaces were highly susceptible to the testing environment at 93°C. The decreasing trend of $R_p$ gradually slowed down and eventually reached a plateau of about 0.16 kΩ cm$^2$ at the end of the 6$^{th}$ day. This trend can be explained by the formation and thickening of a protective oxide scale on the sample surface, which eventually reached dynamic equilibrium. During the experiment of CW 93-50°C, CS samples experienced a considerable rebound in $R_p$ whenever it was subjected to a temperature change from 93 to 50°C, indicating that IW 93°C is more aggressive than IW 50°C for CS samples. This was associated with an increase in the passivation level of the retained oxide film at 50°C. Additionally, this trend can be explained in terms of the concentration of chloride in moisture: i.e., compared to liquid water (at 50°C), water vapor (at 93°C) can more effectively leach out the corrosion species from insulation material. It is worth noting that every temperature change from 50°C to 93°C was accompanied by a significant drop in $R_p$ value. This can be attributed to the alternating formation and decohesion of oxide films due to thermal shock which was later confirmed by the EIS results and corroded surface characterization. Finally, the CW condition led to a higher gradient of decline in average $R_p$ (from 0.36 to 0.08 kΩ cm$^2$) than in the case of IW (from 0.40 to 0.16 kΩ cm$^2$) over the 7 days. This also confirms that the cyclic temperature conditions are more corrosive than the isothermal conditions.

Figure 4(b) illustrates the $R_p$ *vs.* time of SS samples in 3.5 wt% NaCl solutions under IW 93°C and CW 93-50°C conditions. The initial corrosion resistance of SS is significantly higher than that of CS possibly due to the protective chromium oxide film of SS. Because of the high concentration of chloride in moisture, the passivity of SS could be damaged by the breakdown of protective films at the potentials less than the pitting potential [19, 30, 31]. Therefore, the overall decreasing trend of $R_p$ *vs.* time is associated with the corrosion intensified by pitting. It is evident from Figure 4(b) that, whenever SS was subjected to the lower temperature 50°C, the passive chromium film showed higher passivation by exhibiting an $R_p$ rebound. Similar to CS, the decreasing trend for 93°C of CW 93-50°C is much steeper than that of IW 93°C, which indicates that thermal cycling accelerates CUI.

The $R_p$ values were converted into averaged CRs using equations (2) to (4), to be compared with CRs calculated from mass loss data. The averaged CRs were calculated based on the sum of $R_p$ values of 8 points from day 0 to day 7, where the $\overline{R_p}$ values are listed as follows: 0.391 kΩ cm$^2$ for CS-CW, 0.356 kΩ cm$^2$ for CS-IW, 6.616 kΩ cm$^2$ for SS-CW, and 6.395 kΩ cm$^2$ for SS-IW. The averaged CRs

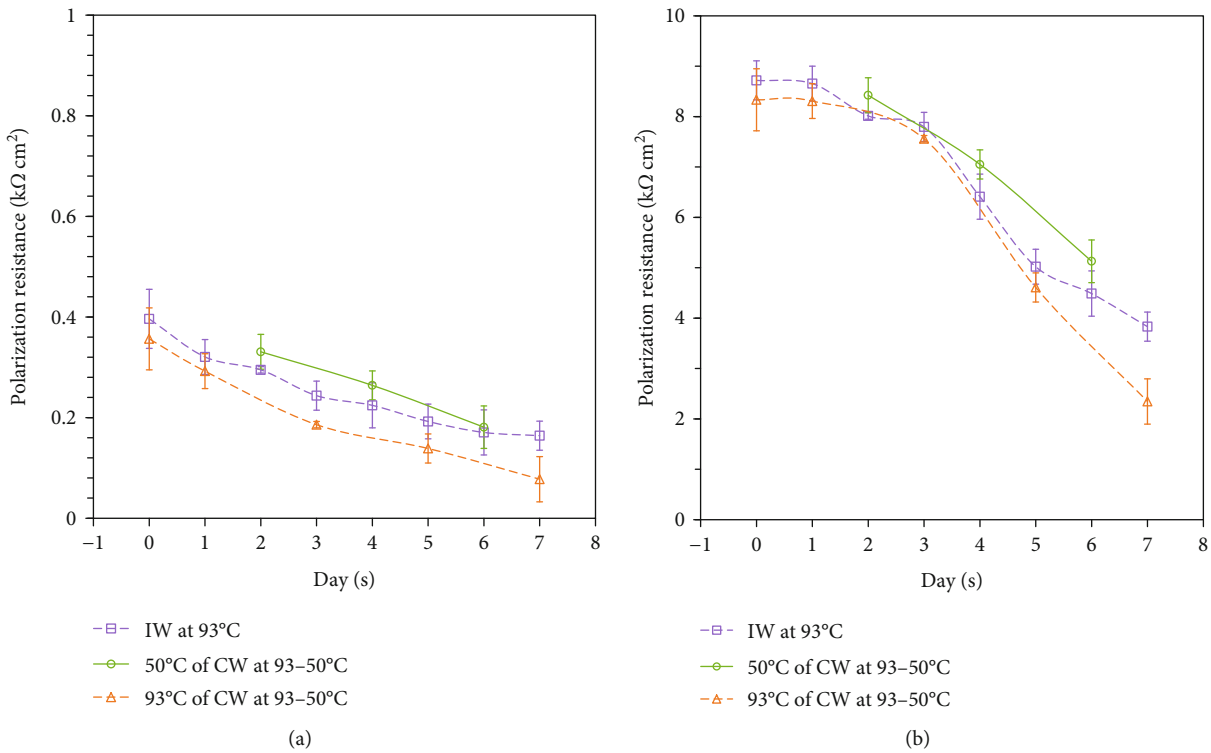


Figure 4: Average polarization resistance ($R_p$) *vs.* time of (a) CS and (b) SS samples in 3.5 wt% NaCl solutions during 7 days.

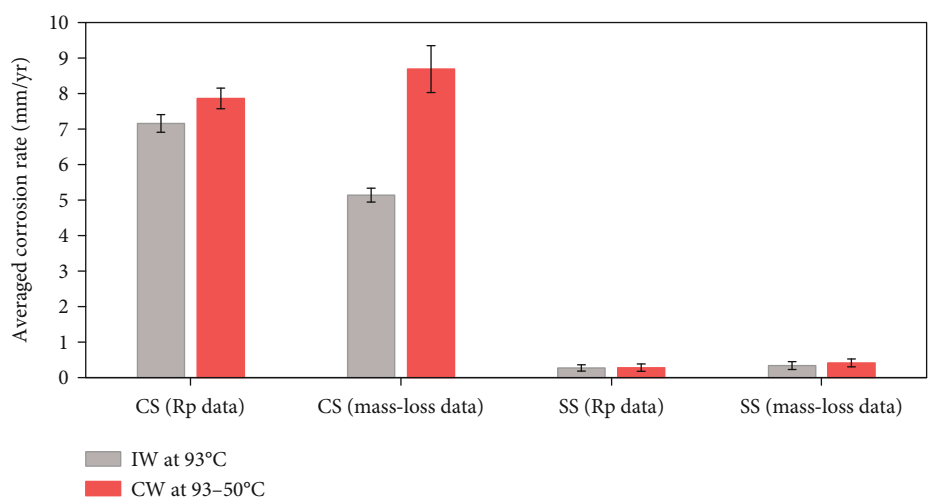


Figure 5: Calculated average CRs of CS and SS samples in 3.5 wt% NaCl solution based on mass loss and polarization resistance ($R_p$) data. Exposure time is 7 days.

calculated from both mass loss and $\overline{R_p}$ values after 7 days of CUI experiments are presented in Figure 5. As expected, SS samples exhibited much better corrosion resistance compared to CS samples [32]. Both CS and SS samples were more severely corroded under CW conditions than under IW conditions. In general, the LPR measurement using the novel electrochemical CUI cell was proven valid, as it can produce comparable CR estimation towards mass loss data.

*3.2.2. Electrochemical Impedance Spectroscopy.* EIS experiments were performed to investigate the surface reactions and properties as a function of exposure time. An EIS experiment was carried out after 1-hour OCP measurement at the end of the 3$^{rd}$, 5$^{th}$, and 7$^{th}$ day of each CUI experiment. Figure 6 presents the Bode plots of CS and SS in 3.5 wt% NaCl solutions during 7-day CW and IW CUI experiments. In Figure 6, all Bode plots changed as a function of the exposure time, which indicates a reaction change on the sample

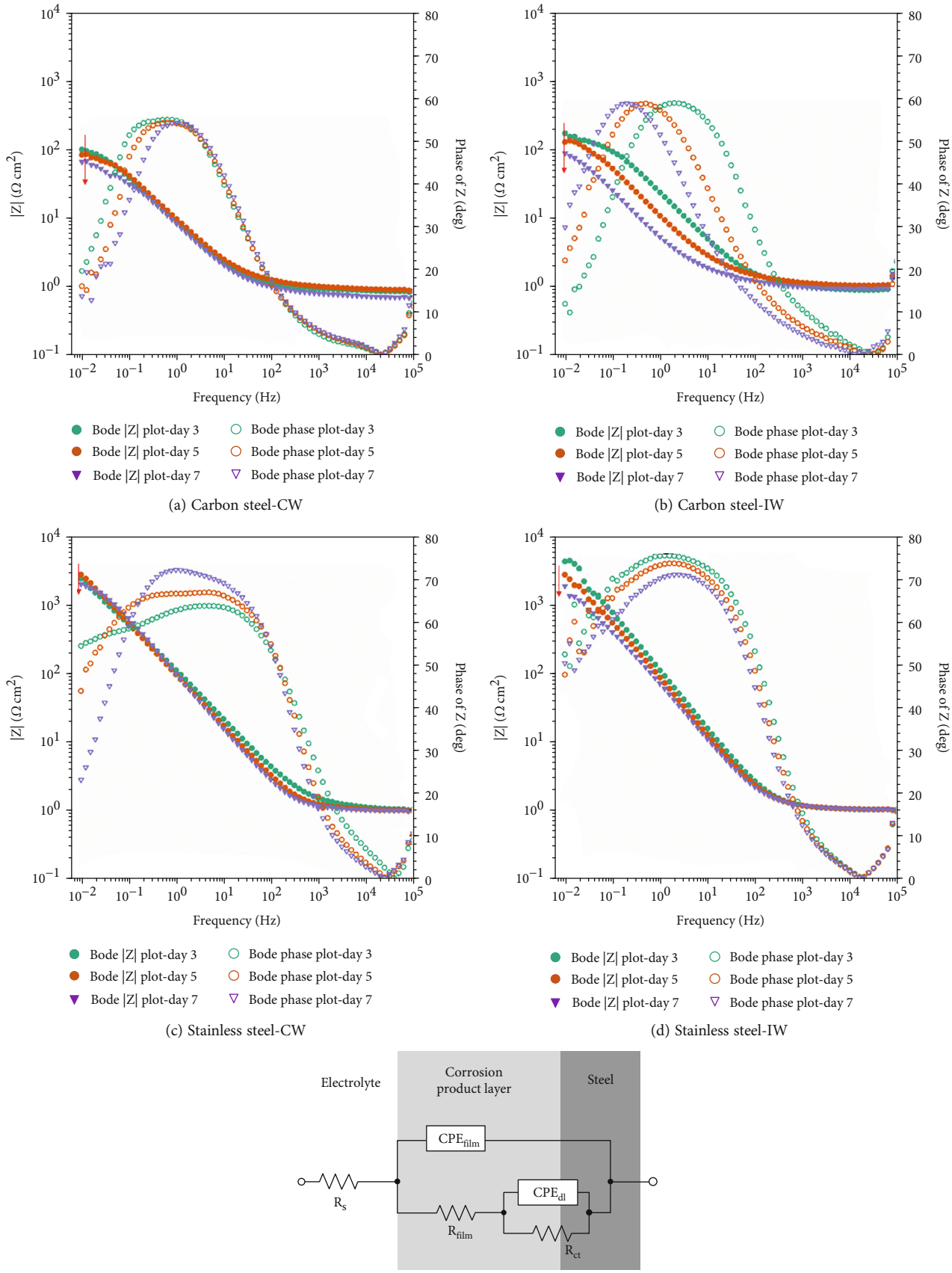


(a) Carbon steel-CW

(b) Carbon steel-IW

(c) Stainless steel-CW

(d) Stainless steel-IW

(e) Equivalent circuit model used to fit all the data

Figure 6: Bode plots of steels in 3.5 wt% NaCl solutions during 7-day CUI experiments as a function of exposure time.

Table 4: Summary of $R_p$ values from LPR and $R_{sol}$, $R_{deposit}$, and $R_{film}$ from EIS measurements for steel samples in 3.5 wt% NaCl solutions during 7 days of CUI experiments.

| | | $R_{sol}$ ($\Omega$ cm$^2$) | | $R_{film}$ ($\Omega$ cm$^2$) | | $R_{ct}$ ($\Omega$ cm$^2$) | | $R_p$ ($\Omega$ cm$^2$) | |
|---|---|---|---|---|---|---|---|---|---|
| | | CS | SS | CS | SS | CS | SS | CS | SS |
| CW | Day 3 | 1.2 | 1.1 | 1.8 | 1640 | 208 | 8493 | 186 | 7560 |
| | Day 5 | 1.2 | 1.1 | 1.0 | 288 | 157 | 4541 | 139 | 4609 |
| | Day 7 | 1.0 | 1.1 | 0.8 | 164 | 116 | 1864 | 78 | 2346 |
| IW | Day 3 | 1.4 | 1.3 | 1.8 | 864 | 307 | 7615 | 244 | 7794 |
| | Day 5 | 1.4 | 1.0 | 1.6 | 190 | 284 | 4941 | 192 | 5019 |
| | Day 7 | 1.4 | 1.0 | 1.5 | 143 | 215 | 3653 | 164 | 3830 |

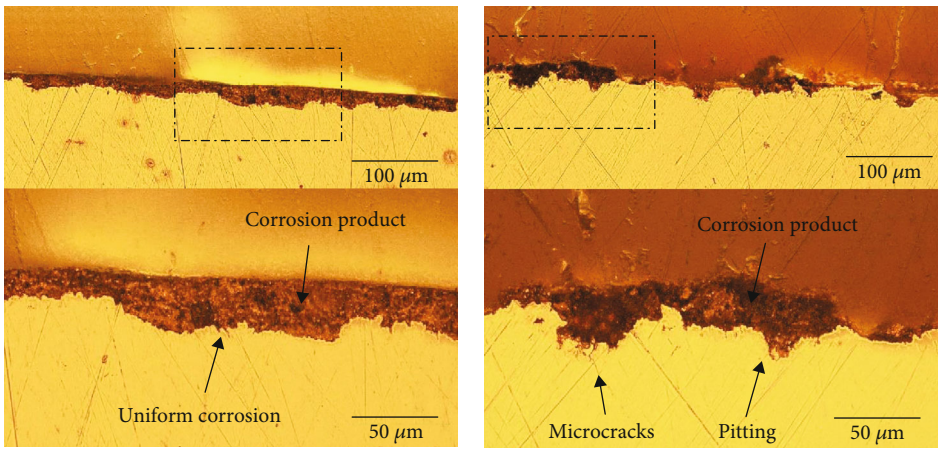


(a) (b)

Figure 7: The cross-sectional surface morphology of CS after CUI tests using 3.5 wt% NaCl solutions for 7 days: (a) IW at 93°C, (b) CW at 93-50°C.

surface. This change can be attributed to local chemistry, surface conditions, and/or corrosion products on the surface. The red arrows show that the magnitude ($|Z|$) of impedance for all 4 experiments decreases from the 3$^{rd}$ to the 7$^{th}$ day. The decreasing impedances agree with the observed $R_p$ trends in Figure 4, indicating an accelerated CR of steels under these testing conditions. In order to obtain more details of the ongoing processes at the interface, EIS data were analyzed by electrical equivalent circuits (EECs).

Many papers have been published on the effects of chloride solutions on steel corrosion [31, 33]. Considering the second phase developed in Figure 6(c), the EECs of $R_{sol}(Q_{ct}R_{ct})$ and $R_{sol}(Q_{film}(R_{film}(Q_{ct}R_{ct})))$ were used, and only $R_{sol}(Q_{film}(R_{film}(Q_{ct}R_{ct})))$ gave the best fitting results for all data. These two EECs include solution resistance ($R_{sol}$), constant-phase element (CPE) behavior for oxide film ($Q_{film}$), oxide film resistance ($R_{film}$), CPE behavior for charge transfer ($Q_{ct}$), and charge transfer resistance ($R_{ct}$). The CPE (symbolized here by $Q$) was used to compensate for the non-ideal behavior of the capacitor [23]. In this work, only the fitting results of various resistances are presented. Table 4 shows that $R_{sol}$ remained relatively unchanged, while $R_{film}$ and $R_{ct}$ of steels all decreased during the exposure in the CUI environments at 93°C. The $|Z|$ of impedance at high frequency corresponds to $R_{sol}$. The small values of the $R_{film}$ for CS over time indicate that the corrosion products on the surface were porous, nonprotective, and easy to peel off. This phenomenon was reported in other publications and was also observed after the setup was disassembled [5, 34]. The decrease in $R_{film}$ of SS can be attributed to the breakdown of protective films formed on the surface. This was later confirmed by surface morphology characterization where pitting corrosion was observed on SS samples. Finally, the decrease in $R_{ct}$ with time was observed in all cases (Table 4), which is in good accord with the trend of $R_p$ obtained from LPR measurements (Figure 4). The values of $R_{ct}$ under the IW conditions are constantly higher than the corresponding values under the CW conditions, except for the $R_{ct}$ on day 3 of SS (CW). This trend further confirms that the CRs of both CS and SS can be accelerated by thermal cycling conditions.

*3.3. Surface Characterization after CUI Experiments.* Figures 7(a) and 7(b) show the cross-sectional morphologies of CS after 7 days of CUI testing with 3.5 wt% NaCl under

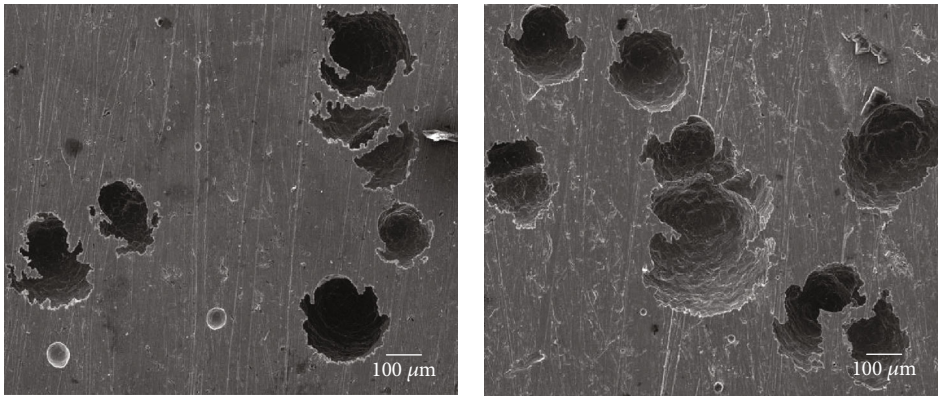


(a) (b)

Figure 8: SEM images of corroded SS after 7 days' CUI tests with 3.5 wt% NaCl solutions. (a) IW at 93°C, (b) CW at 93-50°C.

IW 93°C (Figure 7(a)) and CW 93-50°C (Figure 7(b)) conditions, respectively. Figure 7(a) presents a relatively smooth surface morphology with some wide bumps. The corrosion progression is a more general type (i.e., uniform corrosion) rather than pitting. A layer of corrosion product uniformly covered most of the exposed sample surface [32, 35].

The appearance of surface morphology, corrosion product, and localized attack of tested CS samples from CW condition differed from those of the samples from IW condition. Figure 7(b) shows the obvious pitting in an elliptical and cup shape. In addition, the initiation of certain microcracks at the tip (bottom) of the pits under CW 93-50°C indicates a potential threat of external stress corrosion cracking. The corrosion product from CW condition shows less uniformity and smaller overall thickness than its IW counterpart. Previous EIS analysis has indicated that the corrosion products on the surface were porous and nonprotective. After 7 days of exposure under thermal cycling conditions, large pieces of oxide films fell off and left the bare metal with high oxidation potential. Most of the remaining oxide films were found at the bottom of the pits. This nonuniform deposition of oxide films may induce further differential aeration cells [34], in which regions of the metal surface beneath oxide films are the local anodes, whereas the regions of the exposed surface are the cathodes [20]. This may further accelerate localized corrosion and in turn aggravates the mass loss [20]. Finally, unlike the smooth surface of the corroded sample from IW condition (Figure 7(a)), the surface of CW samples showed more grooves and pits due to the localized corrosion and partially exfoliated corrosion products (Figure 7(b)). These grooves and pits are conducive to the moisture stagnant, which can also lead to more severe mass loss.

Prominent pitting corrosion occurred on SS samples after 7 days of CUI tests. The surface view of corroded samples (SEM images) is shown in Figure 8. The comparison between Figures 8(a) and 8(b) shows no major difference in the morphologies apart from slight variations in pit widths. As discussed in the earlier sections, the passivity of SS is very vulnerable to high concentrations of chloride in moisture making it susceptible to pitting corrosion. Additionally, the previously observed decrease in $R_p$ and $R_{film}$ during the testing days (based on LPR and EIS results) also provided evidence for the protective film breakdown.

## 4. Conclusions

A novel electrochemical CUI cell with three Pt(Ti) wires was developed and used for in situ CUI monitoring and analysis. The CUI behavior of X70 CS and 304 SS samples under four testing conditions (i.e., isothermal/cyclic temperature and wet/dry conditions) was investigated by mass loss, surface characterization, and LPR and EIS measurements. The following conclusions were drawn from this research study:

(1) Isothermal conditions were more aggressive as temperature increased from 50 to 93°C. Cyclic temperature condition is more aggressive than isothermal condition (i.e., CW(D) > IW(D)). On top of the effect of thermal conditions, CS samples corroded faster under cyclic wet-dry than under constant wet with the same thermal conditions, that is, CWD > CW and IWD > IW

(2) LPR data measured using the novel electrochemical technique produced a comparable CR estimation towards mass loss data

(3) The mechanisms behind the accelerated CUI by thermal cycling were revealed by LPR and EIS data. CW led to a higher gradient of reduction in polarization resistance than in the case of IW over the testing period. Furthermore, the oxide film resistance of both CS and SS declined faster under cyclic conditions, suggesting that the corrosion product or film became more porous and nonprotective

(4) The surface characterization illustrated that the accelerated CUI by thermal cycling originates from the deterioration of oxide layers and localized corrosion

(5) The unique Pt(Ti) sensing method has demonstrated its ability to in situ evaluate the resistance and the corrosion rates of substrate materials and/or protective film with time and cyclic temperature. Due to its

accuracy, robustness, and economic advantages, it is practically possible for being installed in petrochemical, refining, offshore, and marine/maritime industries to assist target inspection activities (i.e., on piping, vessels, and tanks). In addition to its potential for real-time CUI monitoring, it could be further applied to rank alloys, coatings, and inhibitors under more complex exposure conditions

## Data Availability

The electrochemical data used to support the findings of this study are available from the corresponding author upon request.

## Conflicts of Interest

The authors declare that they have no conflicts of interest.

## Acknowledgments

The authors gratefully thank Integrity Products & Supplies Inc., Canada, for supplying the insulation materials and Mr. Tom Veret from Université de Technologie de Troyes, France, and Mr. Haohan Chen for their valuable help in CUI experiments.

## References

[1] R. Javaherdashti, "Corrosion under insulation (CUI): a review of essential knowledge and practice," *Journal of Materials Science and Surface Engineering*, vol. 1, no. 2, pp. 36–43, 2014.

[2] P. J. Thomas and J. O. Hellevang, "A distributed fibre optic approach for providing early warning of corrosion under insulation (CUI)," *Journal of Loss Prevention in the Process Industries*, vol. 2020, no. 64, 2020.

[3] P. Roffey and E. H. Davies, "The generation of corrosion under insulation and stress corrosion cracking due to sulphide stress cracking in an austenitic stainless steel hydrocarbon gas pipeline," *Engineering Failure Analysis*, vol. 44, pp. 148–157, 2014.

[4] K. Mizushima, N. Satake, M. Sakai, and J. Miyashita, "Factors for selecting thermal insulation materials to prevent corrosion under insulation," *Corrosion*, vol. 12952, pp. 1–12, 2019.

[5] E. Eltai, K. al-Khalifa, A. al-Ryashi, E. Mahdi, and A. S. Hamouda, "Investigating the corrosion under insulation (CUI) on steel pipe exposed to Arabian Gulf Sea water drops," *Key Engineering Materials*, vol. 689, pp. 148–153, 2016.

[6] NACE International 0198. SP 0198-2010, "Standard recommended practice: the control of corrosion under thermal insulation and fireproofing materials—a systems approach," *NACE Standard RP0198-2010, Item*, vol. 2010, 2010.

[7] J. Reynolds and P. Bock, "Third-generation polysiloxane technology for elevated temperature coatings," in *CORROSION 2018*, pp. 1–12, NACE International, 2018.

[8] Q. Cao, M. Brameld, N. Birbilis, and S. Thomas, "On the mitigation of corrosion under insulation (CUI) of mild steel using local cathodic protection," *Corrosion*, vol. 75, no. 12, pp. 1541–1551, 2019.

[9] N. Tanuma, "What is Optimum Protective Coating System for Cyclic-Temperature Service," in *CORROSION*, pp. 1–13, Phoenix, Arizona, USA, 2018.

[10] S. Caines, F. Khan, J. Shirokoff, and W. Qiu, "Experimental design to study corrosion under insulation in harsh marine environments," *Journal of Loss Prevention in the Process Industries*, vol. 33, pp. 39–51, 2015.

[11] M. Suresh Kumar, M. Sujata, M. A. Venkataswamy, and S. K. Bhaumik, "Failure analysis of a stainless steel pipeline," *Engineering Failure Analysis*, vol. 15, no. 5, pp. 497–504, 2008.

[12] J. W. Lee and K. E. Kee, "Experimental study of chloride-induced stress corrosion cracking (CISCC) for austenitic SUS 304L under thermal insulation2," *Platform: A Journal of Engineering*, vol. 4, pp. 31–43, 2020.

[13] Y. Hou, T. Pojtanabuntoeng, and M. Iannuzzi, "Use of electrochemical current noise method to monitor carbon steel corrosion under mineral wool insulation," *npj Materials Degradation*, vol. 4, no. 1, 2020.

[14] A. Marquez, J. Singh, and C. Maharaj, "Corrosion under insulation examination to prevent failures in equipment at a petrochemical plant," *Journal of Failure Analysis and Prevention*, vol. 21, no. 3, pp. 723–732, 2021.

[15] M. J. Cullin, G. Birmingham, R. Srinivasan, and G. Hailu, "Injectable sodium bentonite inhibitors for corrosion under insulation," *Journal of Pipeline Systems Engineering and Practice*, vol. 11, no. 4, 2020.

[16] ASTM G189-07, "Standard guide for laboratory simulation of corrosion under insulation," Astm. 2008; 07 : 1-11.

[17] E. E. Stansbury and R. A. Buchanan, *Fundamentals of electrochemical corrosion.*, ASM international, Materials Park, Ohio, United States, 2000.

[18] W. G. Ashbaugh, R. D. Kanev, N. Mcgowan, and B. Heimann, "Measurement of Corrosion under Insulation," in *Corrosion97*, OnePetro, 1997.

[19] W. Tian, N. Du, S. Li, S. Chen, and Q. Wu, "Metastable pitting corrosion of 304 stainless steel in 3.5% NaCl solution," *Corrosion Science*, vol. 2014, no. 85, pp. 372–379, 2018.

[20] T. Pojtanabuntoeng, L. L. Machuca, M. Salasi, B. Kinsella, and M. Cooper, "Influence of drain holes in jacketing on corrosion under thermal insulation," *Corrosion*, vol. 71, no. 12, pp. 1511–1520, 2015.

[21] Anon, "Standard practice for preparing, cleaning, and evaluating corrosion test specimens," *ASTM Special Technical Publication*, vol. 90, pp. 505–510, 1985.

[22] Anon, "Standard practice for laboratory immersion corrosion testing of metals," *ASTM Special Technical Publication*, vol. 72, pp. 534–544, 1985.

[23] J. Liu, A. Alfantazi, and E. Asselin, "High temperature corrosion of titanium under conditions relevant to pressure leaching: mass loss and electrochemistry," *Corrosion*, vol. 71, no. 3, pp. 352–366, 2015.

[24] International A, "ASTM G59- standard test method for conducting potentiodynamic polarization resistance measurements," *ASTM International.*, vol. 97, pp. 1–4, 2014.

[25] J. Williams and O. Evans, "The influence of insulation materials on corrosion under insulation," in *NACE Corrosion Conference*, pp. 1–24, Canada, 2010.

[26] H. Liang, J. Liu, R. F. Schaller, and E. Asselin, "A new corrosion mechanism for X100 pipeline steel under oil-covered chloride droplets," *Corrosion*, vol. 74, no. 9, pp. 947–957, 2018.

[27] Q. Cao, M. Esmaily, R. L. Liu, N. Birbilis, and S. Thomas, "Corrosion of mild steel under insulation–the effect of dissolved metal ions," *Corrosion Engineering, Science and Technology*, vol. 55, no. 4, pp. 322–330, 2020.

[28] M. Morcillo, D. De La Fuente, I. Díaz, and H. Cano, "Atmospheric corrosion of mild steel," *Revista de Metalurgia*, vol. 47, no. 5, pp. 426–444, 2011.

[29] E. E. Stansbury, "Effects of aeration on corrosiveness of wet residential building thermal insulation on low carbon steel," *ASTM Special Technical Publication*, vol. 1116, pp. 603–618, 1991.

[30] I. U. Toor, H. M. Irshad, H. M. Badr, and M. A. Samad, "The effect of impingement velocity and angle variation on the erosion corrosion performance of API 5L-X65 carbon steel in a flow loop," *Metals*, vol. 8, no. 6, p. 402, 2018.

[31] A. Pardo, E. Otero, M. C. Merino, M. D. López, M. V. Utrilla, and F. Moreno, "Influence of pH and chloride concentration on the pitting and crevice corrosion behavior of high-alloy stainless steels," *Corrosion*, vol. 56, no. 4, pp. 411–418, 2000.

[32] S. Caines, F. Khan, and J. Shirokoff, "Analysis of pitting corrosion on steel under insulation in marine environments," *Journal of Loss Prevention in the Process Industries*, vol. 26, no. 6, pp. 1466–1483, 2013.

[33] A. Ismail, H. M. Irshad, A. Zeino, and I. H. Toor, "Electrochemical corrosion performance of aromatic functionalized imidazole inhibitor under hydrodynamic conditions on API X65 carbon steel in 1 M HCl solution," *Arabian Journal for Science and Engineering*, vol. 44, no. 6, pp. 5877–5888, 2019.

[34] A. R. K. Rana, M. Yang, J. Umer, T. Veret, and G. Brigham, "Influence of robust drain openings and insulation standoffs on corrosion under insulation behavior of carbon steel," *Corrosion*, vol. 77, no. 6, pp. 681–692, 2021.

[35] M. Shahabi-Navid, M. Esmaily, J.-E. Svensson et al., "NaCl-induced atmospheric corrosion of the MgAl alloy AM50-the influence of $CO_2$," *Journal of the Electrochemical Society*, vol. 161, no. 6, pp. C277–C287, 2014.